

Weak Boson Fusion at 100 TeV

Dorival Gonçalves,¹ Tilman Plehn,² and Jennifer M. Thompson²

¹*PITT-PACC, Department of Physics and Astronomy, University of Pittsburgh, USA*

²*Institut für Theoretische Physik, Universität Heidelberg, Germany*

From the LHC runs we know that, with increasing collider energy, weak-boson-fusion Higgs production dominates as an environment for precision measurements. We show how a future hadron collider performs for three challenging benchmark signatures. Because all of these measurements rely on the tagging jet signature, we first give a comprehensive analysis of weak-boson-fusion kinematics and a proposed two-step jet veto at a 100 TeV hadron collider. We then find this machine to be sensitive to invisible Higgs branching ratios of 0.5%, a second-generation muon Yukawa coupling of 2%, and an enhanced total Higgs width of around 5%, the latter with essentially no model dependence. This kind of performance crucially relies on a sufficient detector coverage and a dedicated weak-boson-fusion trigger channel.

CONTENTS

I. Introduction	2
II. Tagging jets and jet veto	3
III. Higgs to invisibles	7
IV. Higgs to muons	9
V. Off-shell Higgs	11
VI. Summary	15
References	15

I. INTRODUCTION

After the discovery of a light and likely fundamental Higgs boson [1, 2], one of the main goals of particle physics is to test how well the Standard Model describes this particle and its different properties [3]. Beyond the LHC time scale, searches for new physics in the newly discovered Higgs sector are one of the main driving forces behind new colliders. While the expected precision of an e^+e^- Higgs factory has been studied in some detail [4], the corresponding results for a future hadron collider [5, 6] is not yet available. One reason for this is that we expect precision measurements in essentially all standard Higgs channels to be limited by experimental systematics and theoretical uncertainties. A global analysis would simply translate guesses on these two inputs into a highly speculative estimate of the physics reach. On the other hand, we can identify a set of benchmark channels which are not entirely theory or systematics limited. For some of these channels we will illustrate the power of a future hadron collider in Higgs precision studies in this paper.

The physics goals and opportunities of a 100 TeV hadron collider [5–8] with an integrated luminosity around 20 ab^{-1} [9] are currently under intense investigation. A leading pillar of its physics program will be studies of weakly interacting thermal dark matter [10]; it will, for example, be complemented by searches for heavy Higgs bosons [11], studies of the electroweak gauge sector at high energies [12], and tests of the nature of the electroweak phase transition [13]. In the Higgs sector two crucial measurements, which can be reliably studied, are of the top Yukawa coupling [14] and of the triple Higgs coupling [15, 16].

We will ask three additional questions, all of which are related to weak boson fusion production of a SM-like Higgs [17]. This production process is known to be highly efficient at the LHC when combined with standard Higgs decays to tau leptons [18] or to W -bosons [19]. Its theoretical description is more precise than almost any other process at the LHC [20]. The only reason why it played hardly any role in the Higgs discovery was the reduced LHC energy during Run I. Moreover, with these signatures it has been, from the very beginning, at the heart of Higgs precision analyses [21]. A critical ingredient to the success of weak boson fusion as a Higgs production channel is the central jet veto [22]. This removes a large proportion of the QCD backgrounds, which would otherwise overwhelm any analysis. We will discuss it in detail in Sec. II.

First, an invisible Higgs decay to a pair of dark matter particles is not only an obvious channel to search for, it is also very well motivated for example in Higgs portal models [23] and in supersymmetric extensions of the Standard Model [24]. At the LHC we will be able to probe invisible Higgs branching ratios in the few per-cent range [25, 26], and in Sec. III we will see how much better a future hadron collider will be able to do in this decay channel.

Second, the LHC will firmly establish that the Higgs couples to the fermions of the third generation, but the size of the Higgs couplings to the second generation fermions will remain largely unknown. While there are new ideas to measure the Yukawa couplings to second-generation quarks [27], the obvious task is to measure the Higgs branching ratio to muons [28]. We will show in Sec. IV how a 100 TeV collider will turn a proof of the existence of such a coupling into a precise measurement.

Finally, one of the main drawbacks of a hadron collider has always been that it does not allow for a direct measurement of the Higgs width. This changes when we include off-shell Higgs production, for example in the four-lepton final state [29]. The problem with this measurement in gluon fusion is that it relies on the assumption that the effective Higgs-gluon coupling has an energy scaling like in the Standard Model [30]. At a 100 TeV collider we can instead use weak-boson-fusion production with the known, logarithmic scaling given by the renormalization group running of the weak coupling, as we will discuss in Sec. V. A comprehensive analysis of Higgs pair production in weak boson fusion will not be part of our analysis, but can be found in Ref. [16].

II. TAGGING JETS AND JET VETO

A proper understanding and use of the two tagging jets is crucial to any weak boson fusion (WBF) analysis at the LHC or at a future hadron collider. The signal(s) and at least some irreducible backgrounds are independent of the Higgs decay channel, as shown in Fig. 1. Unless otherwise noted, we generate all signal and background events with SHERPA [31], merged up to three jets through the CKKW algorithm [32], and accounting for hadronization effects. The two tagging jet candidates are defined as the two hardest anti- k_T jets with $R = 0.4$ and $p_{T,j} > 40$ GeV, obtained with FASTJET [33]. The full top-mass dependence for gluon-fusion Higgs production is included through re-weighting the effective field theory to the full calculation at each phase-space point. The loop contributions are provided by OPENLOOPS [34]. The scales are set according to the SHERPA METS scale setting algorithm [31].

First, we determine what the WBF signal requirements for the two tagging jets $j_{1,2}$ are [35, 36]. The signal is defined by two high-energetic forward jets going into different hemispheres,

$$\eta_{j_1} \cdot \eta_{j_2} < 0 . \quad (1)$$

The effect of increasing the collider energy from 14 TeV LHC to 100 TeV on the more forward jet rapidity and on the rapidity difference is shown in Fig. 2. Although it would be beneficial to extend the detector coverage from $|\eta_j| < 5$ to $|\eta_j| < 6$ [7, 16], we only require

$$|\eta_j| < 5 \quad (2)$$

and indicate a possible improvement from extending the detector for larger rapidities. In Fig. 2, we observe a shift in the peak of the rapidity difference from $\Delta\eta_{j_1 j_2} = 4.5$ at the LHC to $\Delta\eta_{j_1 j_2} = 5$ for a 100 TeV collider with limited coverage, and to $\Delta\eta_{j_1 j_2} = 5.5$ for all events at larger energy. We will require

$$|\eta_{j_1} - \eta_{j_2}| > 5 , \quad (3)$$

instead of the standard choice $\Delta\eta_{j_1 j_2} > 4.2$ at the LHC [25].

As the second key observable, we show the transverse momenta of the tagging jets in Fig. 3. In contrast to the naive paradigm that a larger hadronic collider energy leads to more and more energetic jets from valence quark scattering, we only observe a modest enhancement on $p_{T,j}$ when we go from LHC energy to 100 TeV. The reason for this is that the typical tagging jet transverse momentum is set by the W and Z -masses and the massive gauge boson splitting kernel. Given a quark with energy E , the probability of finding a collinear jet-boson pair with a boson energy xE

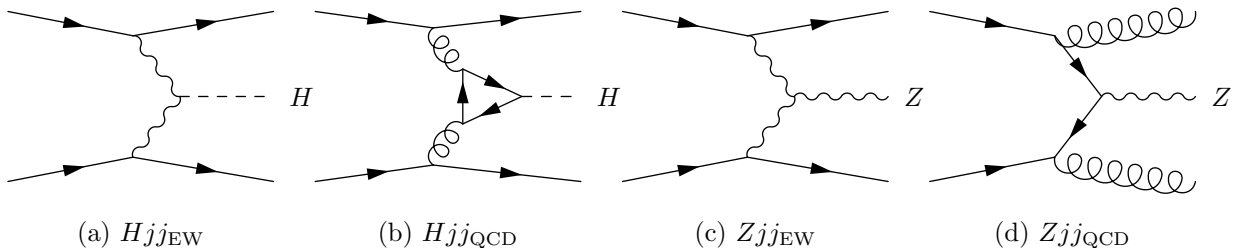


Figure 1: Representative set of Feynman diagrams for the WBF Higgs signal, the contribution from gluon fusion Higgs production, and the two Z +jets backgrounds.

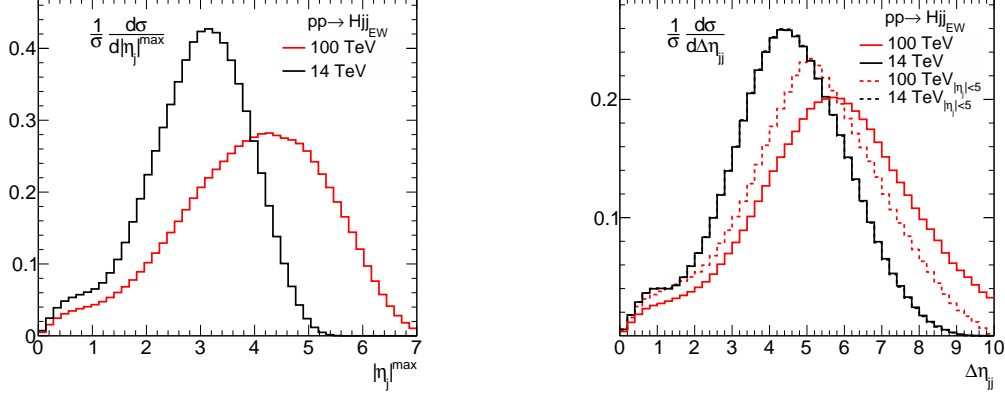


Figure 2: Leading tagging jet rapidity $|\eta_j|^{\max}$ (left) and rapidity difference $\Delta\eta_{j_1j_2}$ (right) for the WBF signal Hjj_{EW} , evaluated at 14 TeV LHC and 100 TeV collider energy. We illustrate the effect of the detector cut $|\eta_j| < 5$ on $\Delta\eta_{j_1j_2}$.

and a transverse momentum p_T is given by [37, 38]

$$P_T(x, p_T) \propto \frac{1 + (1-x)^2}{x} \frac{p_T^3}{(p_T^2 + (1-x)m_V^2)^2},$$

$$P_L(x, p_T) \propto \frac{(1-x)^2}{x} \frac{m_V^2 p_T}{(p_T^2 + (1-x)m_V^2)^2}, \quad (4)$$

where T (L) stands for the transverse (longitudinally) polarized gauge boson V . While for $p_T \ll m_V$ the transverse splitting probability, $P_T(x)$, is suppressed, for $p_T \gg m_V$ the longitudinal splitting probability, $P_L(x)$, decreases faster with increasing p_T . Altogether, this means that kinematic differences between the LHC and a 100 TeV collider are largely limited to the tagging jet rapidities.

The defining feature of any WBF signal at hadron colliders is the suppressed central jet radiation, as compared to the QCD processes illustrated in Fig. 1 [22]. Beyond the usual perturbative QCD arguments, the fundamental reason is the different Poisson vs staircase pattern in the number of radiated jets [39]. In the left panel of Fig. 4, we see how this leads to a reduced jet activity in the signal and can be exploited by a simple jet veto to enhance the signal-to-background ratio to the level of all-electroweak signal and background processes. The samples assume stable Higgs and

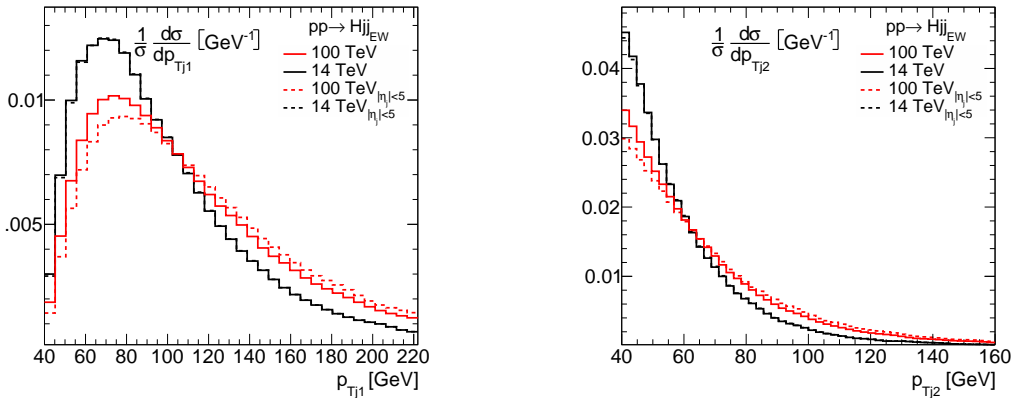


Figure 3: Tagging jet transverse momenta p_{T,j_1} (left) and p_{T,j_2} (right) for the WBF signal Hjj_{EW} .

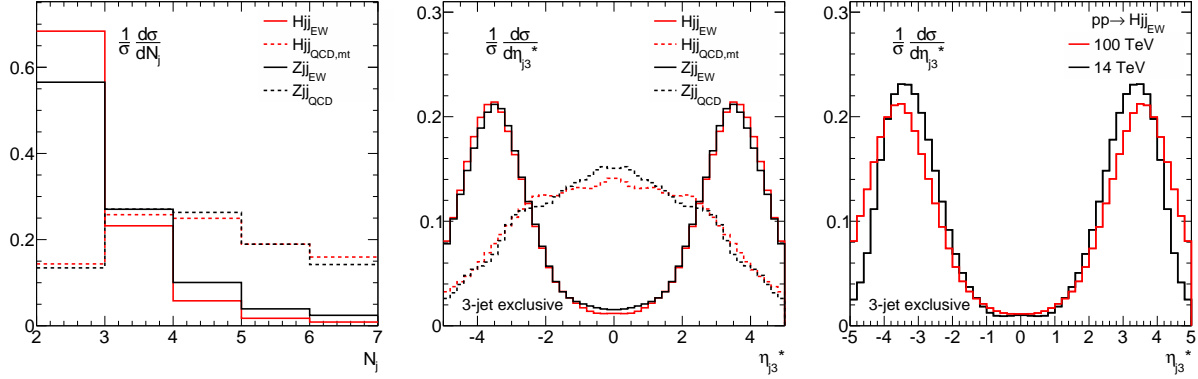


Figure 4: Exclusive number of jets (left) and η_{j3}^* (central and right) distributions for the WBF and the two Zjj backgrounds. In the right panel we do not apply any cut on $|\eta_{j1,2}|$.

Z -bosons, and all jets are defined as anti- k_T jets [33] with $R = 0.4$, $p_{T,j} > 20$ GeV, and $|\eta_j| < 5$. The WBF event selection includes Eqs.(1) and (3), as well as

$$p_{T,j1,2} > 40 \text{ GeV} \quad \text{and} \quad m_{j1j2} > 1200 \text{ GeV} , \quad (5)$$

for the two tagging jets. An obvious question is how much a dedicated analysis of the third jet kinematics can improve over the simple veto [26]. We require this third jet to have a minimum transverse momentum with a default value of

$$p_{T,j3} > p_{T,\text{veto}} = 20 \text{ GeV} . \quad (6)$$

In Fig. 4 we also show the relevant kinematic variable, η_{j3}^* , for which we require

$$\eta_{j3}^* = \eta_{j3} - \frac{\eta_{j1} + \eta_{j2}}{2} > 3 . \quad (7)$$

While the electroweak signal and backgrounds show a suppression for $\eta_{j3}^* = 0$, the QCD background and QCD Higgs production are centered there. We explore these features by defining 2-jet and 3-jet samples by

1. vetoing a third jet for $p_{T,j3} > p_{T,\text{veto}}$;
2. requiring a third jet with $p_{T,j3} > p_{T,\text{veto}}$ and $|\eta_{j3}^*| > 3$, vetoing a fourth jet for $p_{T,j4} > p_{T,\text{veto}}$.

For this two-step strategy it is crucial that we order the jets according to their transverse momenta, *i.e.* the two hardest jet fulfilling our tagging jet criteria are marked as tagging jets. A third, softer jet can then, in principle, be more forward than either of the the tagging jets. Interestingly, the suppression of the central jet activity is even more pronounced at 100 TeV than at the LHC, as shown in the right panel of Fig. 4. Following Fig. 2 the tagging jets have larger rapidities at larger collider energies, so the third jet will follow the tagging jets towards larger rapidities.

The scale above which a fourth jet is vetoed clearly impacts the signal-to-background ratio and on the significance of any Higgs signal. The expectation is for S/B and S/\sqrt{B} to decrease with increasing veto scale, because the QCD-dominated background and signal benefits largely from the increased phase space for additional radiation, whereas the WBF signal does not. Figure 5 shows the signal-to-background ratio for both, the gluon fusion and WBF channels, against the combined QCD and EW Zjj backgrounds. For the WBF signal the ratio decreases as the veto scale

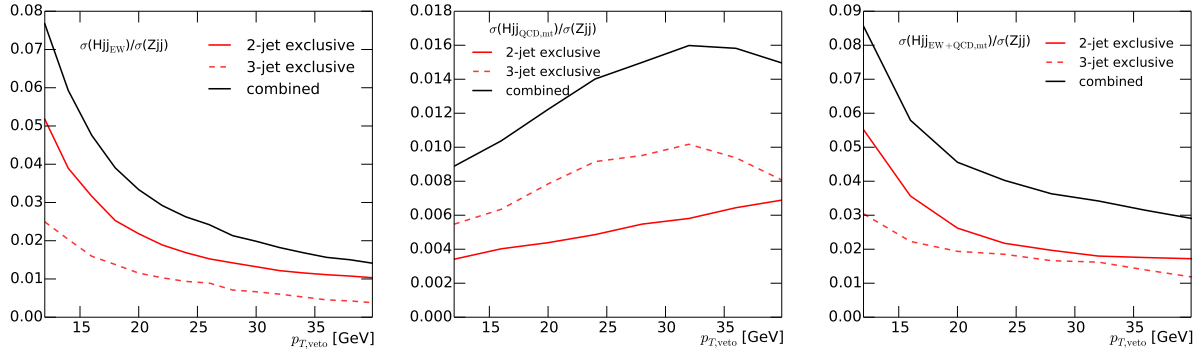


Figure 5: Signal-to-background ratio for WBF production (left), gluon-fusion production (center), and the combined Higgs signal (right) vs dominant QCD and EW Zjj backgrounds. The jet multiplicities are exclusive.

is increased [36]. This behavior can be seen in both the 2-jet and the 3-jet channels. The gluon fusion channel behaves very differently. Because it is a QCD process with Poisson scaling [36], increasing the veto scale increases the sensitivity of the channel. This is a linear increase with the veto scale for the 2-jet channel, while the contribution from the 3-jet channel begins to decrease as it approaches high veto scales. This is because the two leading jets are required to have $p_T > 40$ GeV, so as the third jet p_T is forced to approach this limit there is a reduced phase space for its emission. At this point, with a veto on the fourth jet above $p_{T,j} > 40$ GeV, the signal sample consists of 1/3 gluon fusion events, even after WBF cuts.

In the right panel of Fig. 5 we show the signal-to-background ratio for the combined Higgs signal. The 2-jet channel shows a flattening behavior at veto scales above 30 GeV. The 3-jet channel behaves more in line with expectations, and the signal-to-background ratio slowly decreases with veto scale. Combining the two channels leads to a decrease in the ratio in the range we study. Throughout this paper we use a default veto scale of $p_{T,\text{veto}} = 20$ GeV. This choice of veto scale is identical to the scale which separates the 2-jet and 3-jets samples, as defined in Eq.(6). If the p_T requirement for the tagging jets were higher and the 3-jet significance for the gluon fusion channel did not fall off so quickly, the sensitivity in the high veto scale region could even increase.

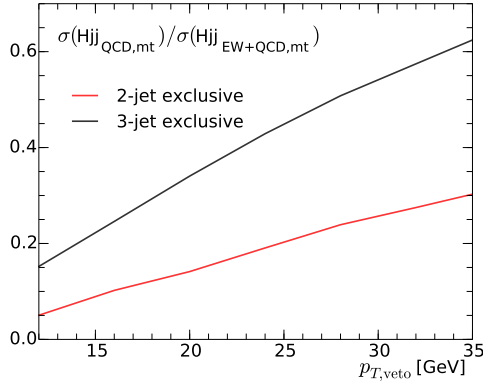


Figure 6: Fractions of gluon fusion events in the Higgs signal after WBF cuts, as a function of the veto scale for the fourth jet.

This effect is also present, and to a slightly larger extent, in a signal over square-root background analysis.

In Fig. 6 we show how the fraction of gluon fusion events in the Higgs signal changes with the jet veto scale, after applying the usual WBF cuts. The range of veto scales is limited by the tagging jet requirement $p_{T,j_{1,2}} > 40$ GeV. The exclusive 3-jet rate with our two-step veto strategy dominates the analysis power and for realistic veto scales of $p_{T,\text{veto}} = 20 \dots 35$ GeV, the gluon fusion contamination varies between 15% and 30% for the 2-jet channel and between 35% and 60% for the 3-jet channel. This kind of analysis should eventually allow us to reduce our dependence on Monte Carlo predictions and separate the two Higgs production processes based on data.

III. HIGGS TO INVISIBLES

For a first analysis making use of tagging jets at a 100 TeV collider, we turn to Higgs decays to invisible particles [25, 26], where the corresponding branching ratio $\text{BR}(H \rightarrow \text{inv})$ is part of modern global Higgs coupling analyses [40]. The main backgrounds are Zjj and Wjj production, as illustrated in Fig. 1. At the level of our analysis detector effects, aside from acceptance cuts, should not play any noticeable role. The only exception is the missing transverse momentum measurement, for which we include a gaussian smearing of $\Delta \cancel{E}_T = 20$ GeV.

We start our analysis requiring two tagging jets with

$$\eta_{j_1} \cdot \eta_{j_2} < 0 \quad p_{T,j_{1,2}} > 40 \text{ GeV} \quad |\eta_{j_{1,2}}| < 5 \quad \Delta\eta_{j_1 j_2} > 5. \quad (8)$$

Following the original analysis [25] we apply an additional cut on the azimuthal angle between the tagging jets

$$\Delta\phi_{j_1 j_2} < 1, \quad (9)$$

which is sensitive to the Lorentz structure of the hard interaction [41].

Our two-step central jet veto is based on Eqs.(6) and (7). In addition, we veto any isolated lepton where the isolation criterion requires less than 20% of hadronic activity in a radius $R = 0.2$

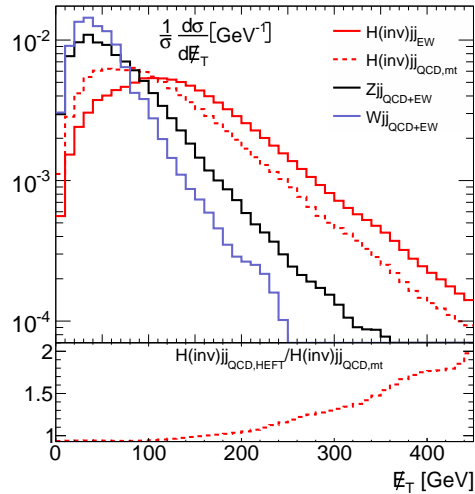


Figure 7: Missing transverse energy distribution \cancel{E}_T for signal and backgrounds. The bottom panel displays the ratio between the heavy-top approximation and the correct result for the QCD Higgs production process.

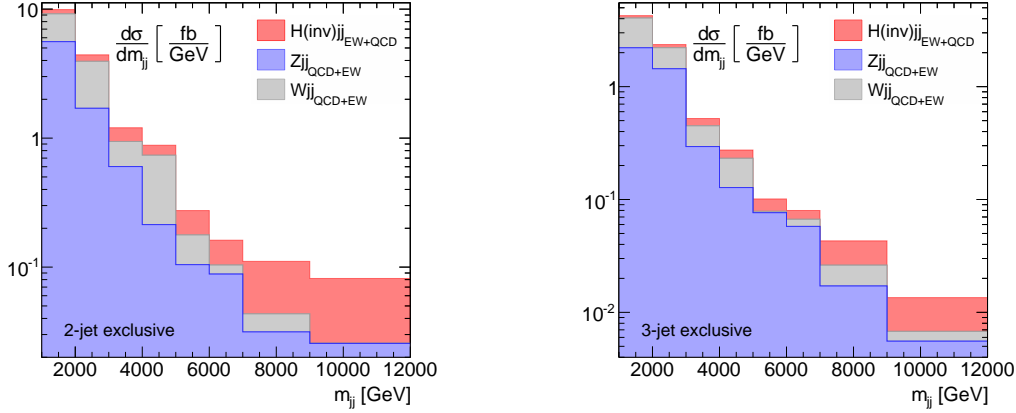


Figure 8: Stacked invariant mass distribution $m_{j_1j_2}$ for the two tagging jets, separated for the exclusive 2-jet (left) and 3-jet (right) samples.

around the lepton. This requirement is shown to be very efficient in suppressing the W +jets background.

In Fig. 7, we display the normalized \cancel{E}_T distributions for the two Higgs channels and the backgrounds. In the bottom panel we show how the heavy-top approximation for this channel fails towards large missing energies $\cancel{E}_T \gtrsim m_t$ [42, 43]. Clearly, any measurement including a missing transverse energy cut needs to account for the full top mass dependence. Because both backgrounds peak around $\cancel{E}_T = 40$ GeV and the gluon fusion Higgs channel peaks around $\cancel{E}_T = 60$ GeV, for the extraction of the WBF signal we require

$$\cancel{E}_T > 100 \text{ GeV} . \quad (10)$$

After applying all cuts we arrive at the invariant mass distributions of the tagging jets shown in Fig. 8. While we have confirmed that the transverse momentum spectrum does not significantly change when we go from the LHC to 100 TeV, this is obviously not true for the longitudinal momenta or the invariant mass of the tagging jets. The regime sensitive to the WBF Higgs signal at 100 TeV starts only around $m_{j_1j_2} \gtrsim 7$ TeV, indicated by a signal-to-background ratio around one. For our estimate of the collider reach we rely on the three kinematic observables

$$\{ \cancel{E}_T, m_{j_1j_2}, N_j \} , \quad (11)$$

within their allowed range $\cancel{E}_T > 100$ GeV and $N_j = 2, 3$. They are chosen to include information on the tagging jets $(m_{j_1j_2}, N_j)$, as well as everything we know about the Higgs momentum (\cancel{E}_T).

To estimate the constraining power on $\text{BR}(H \rightarrow \text{inv})$, we perform a three-dimensional binned log-likelihood analysis for CL_s based on the vector of kinematic distributions shown in Eq.(11). It exploits the rate and the shape information in the two panels of Fig. 8, combined with the \cancel{E}_T dependence. For an early running with an integrated luminosity of 10 fb^{-1} we use the systematic uncertainties from the CMS mono-jet search [44], where the systematics for $Z \rightarrow \nu\nu$ and $W \rightarrow \ell\nu$ backgrounds range around 5% on the background rate. These uncertainties are modeled as nuisance parameters. For the target luminosity of 20 ab^{-1} we assume these uncertainties to reach 0.5%, hoping for a better understanding of the systematic uncertainties with more data. This is significantly worse than the scaled luminosity would suggest, so all of our results will be systematics limited.

In the left panel of Fig. 9 we show the expected 95% CL bound on $\text{BR}(H \rightarrow \text{inv})$ as a function

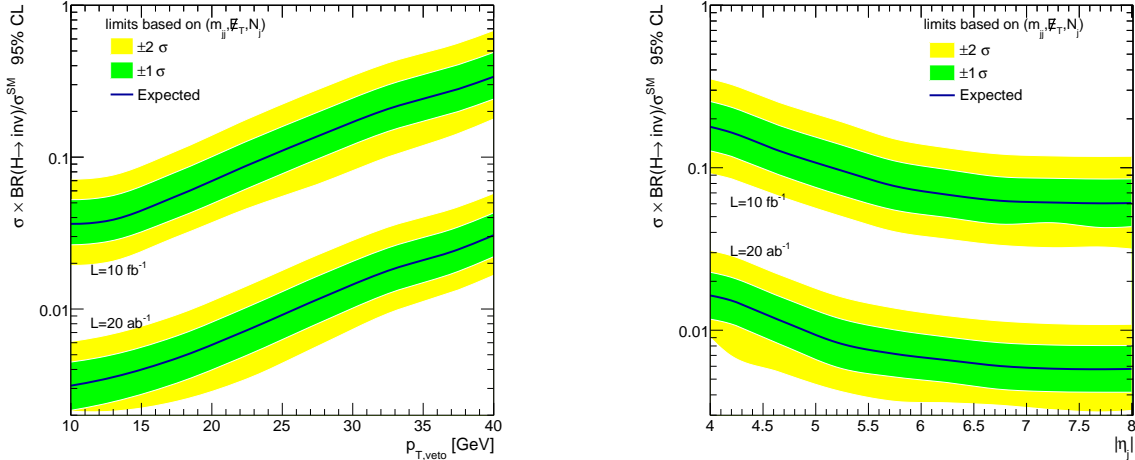


Figure 9: Expected 95% CL bound on the invisible Higgs branching ratio, based on a log-likelihood analysis of the three-dimensional distribution $\{\cancel{E}_T, m_{jj}, N_j\}$. We vary the $p_{T,\text{veto}}$ with $p_{T,j_3} > p_{T,\text{veto}}$ (left) and the maximum rapidity $|\eta_j|$ (right).

of the minimum transverse energy of the third jet, keeping the two tagging jets at $p_{T,j_{1,2}} > 40$ GeV and the detector coverage at $|\eta_j| < 5$. A reduced third jet threshold will enhance the effect of our analysis of the third jet kinematics [26]. Even using track jets or even objects without a jet reconstruction, we do not expect to be able to go below 10 GeV, because of underlying event and pile-up. The experimental challenge in searching for invisible Higgs decays turns out to be the same as for dark matter searches [10]; we need to increase the collider energy while at the same time keeping the detector thresholds as low as possible.

In the right panel of Fig. 9, we estimate the impact of the rapidity coverage for the two tagging jets. The threshold for the third jet is kept at $p_{T,j_3} > 30$ GeV. As expected from Fig. 2, there are only minor gains if we extend the detector range past $|\eta_j| \sim 6$. Altogether, we find that with an excellent detector performance and similarly good control of the systematics a reach of

$$\text{BR}(H \rightarrow \text{inv}) \lesssim 0.5\% \quad (12)$$

for a Standard Model production rate appears to be realistic at a 100 TeV machine. However, as mentioned before, any number below one per-cent strongly relies on our assumptions on background systematics.

IV. HIGGS TO MUONS

As a second benchmark process to illustrate WBF Higgs production at 100 TeV, we consider the decay to second-generation leptons $H \rightarrow \mu^+ \mu^-$. This decay channel will barely be observable at the LHC, and will hardly lead to a precise measurement of the muon Yukawa coupling in the Standard Model [28]. The dominant Zjj backgrounds are illustrated in Fig. 1. In addition, we consider off-shell di-boson and $t\bar{t}$ backgrounds, denoted as $\mu^+ \mu^- \nu \bar{\nu} jj$. Their effect is very small.

We employ a very similar analysis to the invisible Higgs search. The tagging jets are defined according to Eqs.(8) and (9) and combined with the two-step jet veto defined in Eqs.(6) and (7) to control the $t\bar{t}$ and QCD Zjj backgrounds. In addition, we require a maximum amount of missing transverse energy, $\cancel{E}_T < 40$ GeV. For the exclusive 2-jet and 3-jet samples we show the transverse momentum of the muon pair in Fig. 10, as one example distribution. It illustrates how, just based

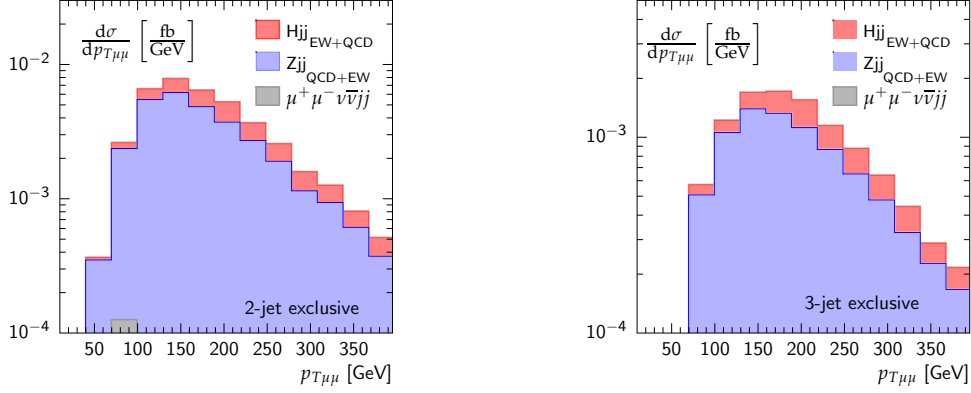


Figure 10: Stacked transverse momentum distribution for the $\mu\mu$ system for the exclusive 2-jet (left) and 3-jet (right) samples. We require an invariant mass window $|m_{\mu\mu} - m_H| < 5$ GeV.

on a few kinematic cuts, we will not be able to extract the Higgs signal efficiently [28]. Even at a 100 TeV collider, the search for Higgs decays to muons will be a multi-variate problem.

One of the ingredients to our analysis will still be a data-driven side band analysis of the $m_{\mu\mu}$ distribution, searching for a narrow Higgs peak. The stacked signal and background distribution is shown in Fig. 11, for two hypothetical experimental resolutions on the muon transverse momentum, $\delta p_{T\mu}/p_{T\mu} = 0.5\%$ and 1% . The muon energy scale uncertainty directly impacts in the invariant mass resolution. At the LHC, the typical transverse momentum uncertainty is $\delta p_{T\mu}/p_{T\mu} \approx 1 \dots 2\%$ for $p_{T\mu} = 20 \dots 100$ GeV [45].

As for the invisible Higgs, we again derive the sensitivity of a 100 TeV collider in the exclusive 2-jet and 3-jet bins shown in Fig. 11. Similar to Eq.(11), we exploit the three kinematic observables

$$\{ m_{\mu\mu}, m_{j_1 j_2}, N_j \}, \quad (13)$$

where the information on the Higgs resonance is encoded in $m_{\mu\mu}$. We show the resulting 95% CL sensitivity as a function of the integrated luminosity in Fig. 12. To quantify the possible gains in sensitivity from a better muon momentum resolution, we again display two hypothetical experimental uncertainties on the muon transverse momentum, $\delta p_{T\mu}/p_{T\mu} = 0.5, 1\%$, to be achieved at

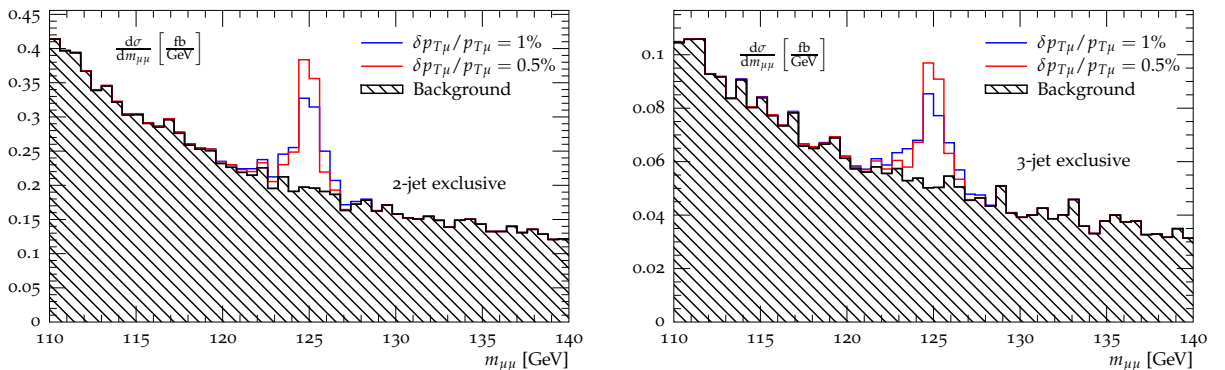


Figure 11: Stacked invariant mass distribution $m_{\mu\mu}$ for the 2-jet (left) and 3-jet (right) exclusive samples. We display results for two uncertainties $\delta p_{T\mu}/p_{T\mu} = 0.5\%$ and 1% .

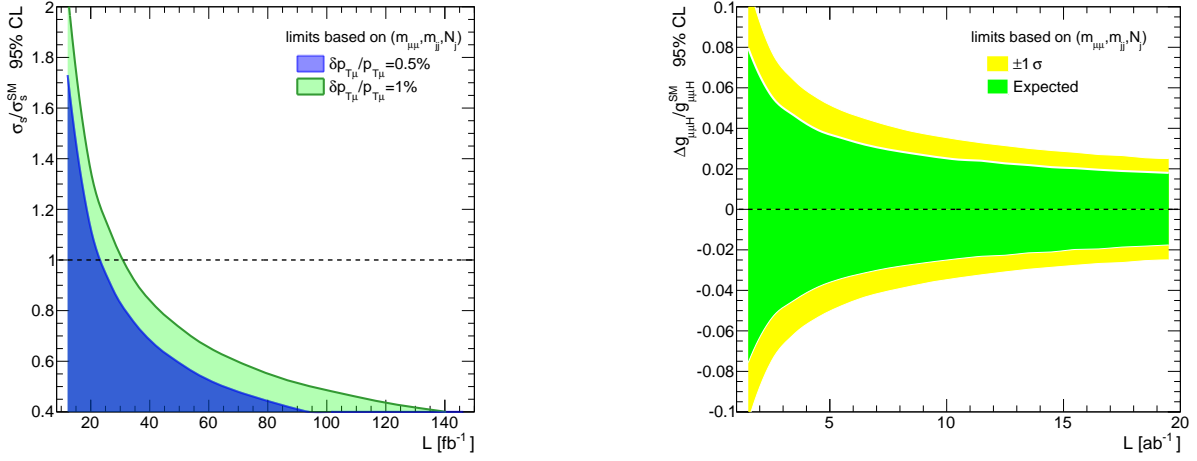


Figure 12: Expected 95% CL bound on the signal strength $\sigma_s/\sigma_s^{\text{SM}}$ (left) and on the muon coupling $\Delta g_{\mu\mu H}/g_{\mu\mu H}^{\text{SM}}$ (right) as a function of the integrated luminosity. We employ a log-likelihood analysis of the three-dimensional distribution $\{m_{\mu\mu}, m_{j_1 j_2}, N_j\}$. For the left panel we assume two experimental uncertainties for the muon reconstruction, in the right panel we fix $\delta p_{T\mu}/p_{T\mu} = 0.5\%$.

a 100 TeV collider. We conclude that it is possible to see the $H \rightarrow \mu^+ \mu^-$ channel at 95% CL with $\mathcal{L} \lesssim 40 \text{ fb}^{-1}$ for both uncertainty scenarios. Moreover, we will be able to measure the muon coupling to

$$\frac{\Delta g_{\mu\mu H}}{g_{\mu\mu H}^{\text{SM}}} \lesssim 2\% , \quad (14)$$

assuming a Standard Model production rate and an integrated luminosity of $\mathcal{L} = 20 \text{ ab}^{-1}$.

V. OFF-SHELL HIGGS

Measuring off-shell production rates for a Higgs boson decaying to four fermions targets a major shortcoming of any hadron collider by giving us a handle on the total Higgs width [29, 46]. The dominant LHC channel, $gg \rightarrow H^* \rightarrow 4\ell$, is not well-suited for such a measurement, because the gluon-Higgs coupling is loop-induced. This implies that the dependence of the coupling has a complex dependence on the incoming and outgoing momenta, determined by the underlying particle content [30]. Any global analysis using off-shell rate measurements has to be based on a well-defined hypothesis [40]. If we define such a hypothesis for the Higgs-top-gluon Lagrangian the off-shell measurements can be naturally combined with boosted Higgs production [43].

The WBF production channel involves only renormalizable tree-level Higgs couplings, which we know run logarithmically using the usual renormalization group equation. Unlike the two WBF Higgs signatures discussed before, off-shell production in weak boson fusion is unlikely to be seen at the LHC altogether [29, 30].

At a 100 TeV collider we expect a sizeable event sample for $pp \rightarrow H jj_{\text{EW}} \rightarrow (4\ell) jj$, even for off-shell Higgs production with $m_{4\ell} \gg m_H$. The dominant backgrounds are $ZZjj_{\text{QCD}}$ and $ZZjj_{\text{EW}}$ production, illustrated in Fig. 13. There is an interference between the EW and QCD amplitudes, but it is color suppressed and has been shown to be negligible for total rates and for distributions after the WBF cuts [47]. As always, the QCD background can be suppressed by the standard

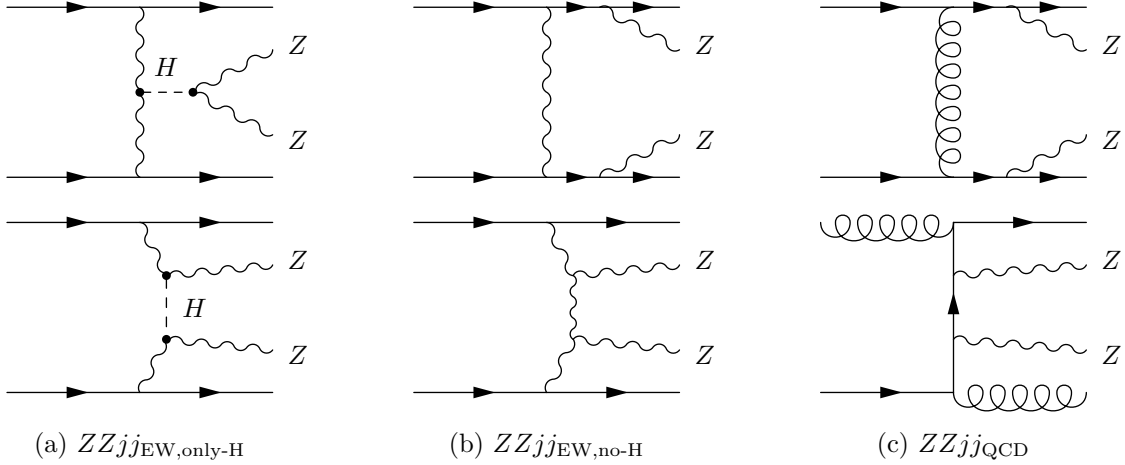


Figure 13: Representative set of Feynman diagrams for WBF $ZZjj$ production through a Higgs (left), in an electroweak process (center), and including the strong interaction (right).

WBF cuts and a central jet veto. Unlike for on-shell Higgs decays, the EW background helps our analysis through its interference with the Higgs diagrams. We generate the signal and background samples with MADGRAPH5+PYTHIA8 [48, 49] and observe good agreement with MCFM [50]. Spin correlations and off-shell effects are fully accounted for, including the Z -decays.

We start by requiring four isolated leptons with less than 15% of the hadronic activity within a radius of $R = 0.2$. The kinematic selection follows the CMS analysis [46],

$$\begin{aligned}
 p_{T\ell} &> 5 \text{ GeV} & |\eta_\ell| &< 2.5 & m_{4\ell} &> 100 \text{ GeV} \\
 m_{\ell\ell'} &> 4 \text{ GeV} & m_{\ell\ell,1} &= [40, 120] \text{ GeV} & m_{\ell\ell,2} &= [12, 120] \text{ GeV} .
 \end{aligned} \tag{15}$$

The two $m_{\ell\ell}$ ranges define a leading and a sub-leading flavor-matched lepton pair. For the tagging jets we again require Eq.(8), combined with $m_{j_1 j_2} > 600 \text{ GeV}$ and our two-step jet veto based on Eqs.(6) and (7).

Building on the tagging jet kinematics discussed in Sec. II, we show the tagging jet rapidities for three slices of $m_{4\ell}$ in Fig. 14. For more off-shell Higgs production, the tagging jets move further into the forward region. This behavior is related to gauge boson scattering, $VV \rightarrow VV$, at high energies. The off-shell phase space region provides the ideal setup for the effective W/Z -approximation, where the vector boson parton picture requires a hierarchy of energy scale, $\sqrt{s} \gg m_{4\ell} \gg m_V$. Here, the longitudinal and transverse scattering amplitudes scale as $\mathcal{A}_{LL}/\mathcal{A}_{TT} \sim m_{4\ell}^2/m_V^2$. This feature is more prominent at 100 TeV than at 14 TeV collider energy because at larger scattering energies we produce a greater fraction of longitudinal gauge boson even at the Higgs pole [38], see Fig. 2. We can use this feature by increasing the $\Delta\eta_{j_1 j_2}$ cut for the off-shell analysis, indicating that a detector coverage to rapidities larger than $|\eta_j| = 5$ will be even more important than in other WBF channels.

In what follows, we will assume that the Higgs couplings to W and Z gauge bosons change simultaneously as $g_{ZZH}/g_{ZZH}^{\text{SM}} = g_{WWH}/g_{WWH}^{\text{SM}}$, respecting custodial symmetry. We can then write the $ZZjj_{EW}$ amplitude as the sum of the $ZZjj_{EW,only-H}$ and $ZZjj_{EW,no-H}$ contributions,

$$\mathcal{A}_{EW} = \left(\frac{g_{ZZH}}{g_{ZZH}^{\text{SM}}} \right)^2 \mathcal{A}_H + \mathcal{A}_B , \tag{16}$$

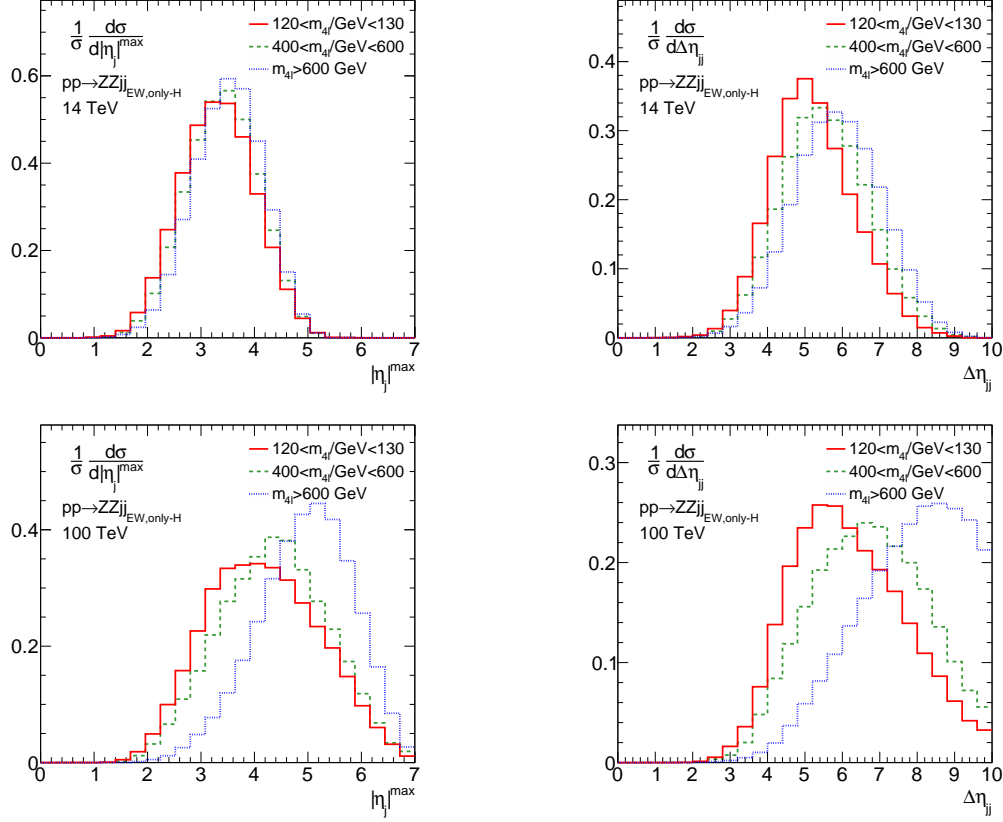


Figure 14: Leading tagging jet rapidity (left) and rapidity difference (right) for $ZZjj_{EW,only-H}$ signal at 14 TeV (top) and 100 TeV (bottom). We show three phase space regions not requiring the standard cuts $|\eta_{j1,2}| < 5$ and $\Delta\eta_{jj} > 5$.

where \mathcal{A}_H corresponds to Fig. 13(a) and \mathcal{A}_B corresponds to Fig. 13(b). Following this notation, any observable distribution can be decomposed as

$$\frac{d\sigma_{EW}}{d\mathcal{O}} = \left(\frac{g_{ZZH}}{g_{ZZH}^{SM}}\right)^4 \frac{d\sigma_{HH}}{d\mathcal{O}} + \left(\frac{g_{ZZH}}{g_{ZZH}^{SM}}\right)^2 \frac{d\sigma_{HB}}{d\mathcal{O}} + \frac{d\sigma_{BB}}{d\mathcal{O}}. \quad (17)$$

While any measurement of an on-shell Higgs signal rate has a flat direction if we vary the involved Higgs couplings together with the total Higgs width, the above measurement will allow us to break this degeneracy and derive a bound on Γ_H .

In Fig. 15 we show the $m_{4\ell}$ distribution for the signal and backgrounds at 14 TeV (left) and 100 TeV (right). First, we observe that the QCD background, $ZZjj_{QCD}$, is depleted by our selections, leaving $ZZjj_{EW}$ as the leading background. Secondly, the interference between the $ZZjj_{EW,only-H}$ signal and the background $ZZjj_{EW,no-H}$ is large and destructive. This leads to a smaller full $ZZjj_{EW,full}$ rate than the Higgs signal alone in the far off-shell regime. Finally, the signal distribution at 100 TeV presents a significantly smaller slope than at the LHC, related to the stronger longitudinal gauge boson polarization at larger energies.

Again, we derive our bound on the measured total Higgs with in terms of Γ_H/Γ_H^{SM} through a log-likelihood analysis. While the Higgs width can be either smaller or larger than the SM prediction, the more interesting question is how we can constrain additional, unobserved Higgs decay channels, leading to an increase in the width, $\Gamma_H/\Gamma_H^{SM} > 1$. Because the signal and the

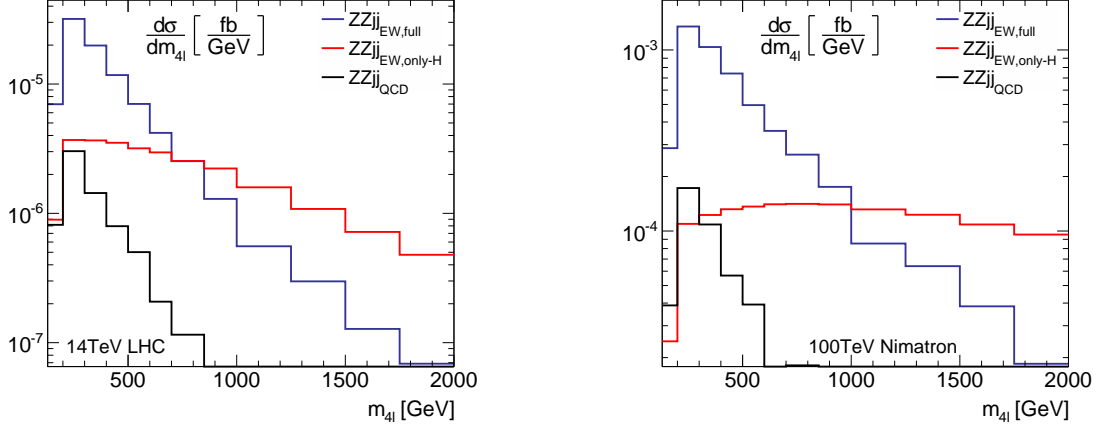


Figure 15: $m_{4\ell}$ distributions for the Higgs signal and the different backgrounds at 14 TeV (left) and 100 TeV (right). We require $\Delta\eta_{j_1j_2} > 6$ to enhance the signature.

leading background are both electroweak, we do not need to include N_j as part of this analysis. In addition, following the above arguments we replace $m_{j_1j_2}$ from the previous analyses in Eq.(11) and (13) by $\Delta\eta_{j_1j_2}$, giving us a likelihood distribution over

$$\{m_{4\ell}, \Delta\eta_{j_1j_2}\}. \quad (18)$$

For consistency, we discard events with $m_{4\ell} > 2$ TeV to avoid gathering sensitivity from unitarity-violating theory predictions [51]. Our projected reach and the associated uncertainties are displayed as a function of the rapidity coverage in Fig. 16. We find that a 100 TeV collider will be sensitive to

$$\frac{\Gamma_H}{\Gamma_H^{\text{SM}}} > \begin{cases} 1.08 & \text{for } |\eta_j| < 5 \\ 1.04 & \text{for } |\eta_j| < 6.5, \end{cases}$$

assuming a Standard Model production rate and an integrated luminosity of $\mathcal{L} = 20 \text{ ab}^{-1}$.

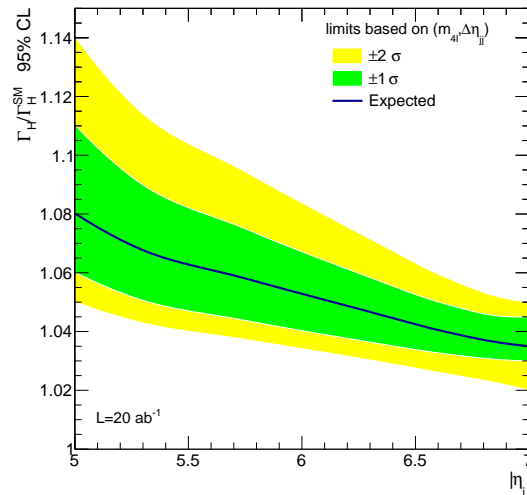


Figure 16: Expected 95% bound on the total Higgs width, based on a log-likelihood analysis of the two-dimensional distribution $\{m_{4\ell}, \Delta\eta_{j_1j_2}\}$.

VI. SUMMARY

We have systematically studied Higgs production in weak boson fusion at a future 100 TeV hadron collider. This signature is crucial for global analyses of the Higgs sector and gives us access to non-trivial Higgs properties. We started with an analysis of the tagging jet kinematics, indicating that it would be beneficial to extend the calorimeter coverage to rapidities $\eta_j \approx 6$. A central jet analysis significantly reduced all QCD backgrounds and ensured that the dominant Higgs signal at a 100 TeV hadron collider is from weak boson fusion. We advertize a two-step veto, where a third jet in between the two tagging jets is kinematically analyzed, while a fourth jet is vetoed. The details of the tagging jet kinematics and the rate dependence on the jet veto scale will allow us to reduce the dependence of WBF rate measurements from Monte Carlo simulations.

Instead of a global Higgs couplings analysis, where most underlying rate measurements at 100 TeV will be systematics or theory limited and the quantitative results will be just guess work, we studied three particularly challenging WBF benchmark signatures.

First, we studied Higgs decays to invisible states, for example dark matter candidates in Higgs portal models. We found that, depending on experimental systematics, we can test invisible Higgs decays with a branching ratio from one per-cent to one per-mille at a 100 TeV collider with an integrated luminosity of 20 ab^{-1} . The key challenge in this analysis, as well as in the corresponding HL-LHC analysis, is our understanding of the central hadronic activity [26].

Next, we determined the reach of a 100 TeV collider in measuring the muon Yukawa coupling. This analysis rests on our ability to separate the kinematically similar Z -decays to muon pairs from the Higgs signal. A precision measurement of the muon Yukawa coupling, assuming a Standard Model production cross section, should be at the level of 2%.

Finally, we considered a measurement of the total Higgs width through off-shell Higgs production in weak boson fusion. Unlike gluon fusion production, this signature does not have a significant model dependence, because the underlying coupling appears at tree level and is therefore renormalizable. We find that a 100 TeV will be able to detect an enhancement of the total Higgs width by around 5%.

All of these Higgs precision analyses will hugely benefit from dedicated WBF triggers and an increased tagging jet rapidity coverage at a 100 TeV collider. Under realistic assumptions the WBF processes should allow us to systematically study electroweak processes at an energy-frontier hadron collider.

Acknowledgments

DG was funded by U.S. National Science Foundation under the grant PHY-1519175. JT is supported by the *Bundesministerium fr Bildung und Forschung* (BMBF Grant No. 05H15VHCA1).

-
- [1] P. W. Higgs, Phys. Lett. **12**, 132 (1964); P. W. Higgs, Phys. Rev. Lett. **13**, 508 (1964); F. Englert and R. Brout, Phys. Rev. Lett. **13**, 321 (1964).
 - [2] G. Aad *et al.* [ATLAS Collaboration], Phys. Lett. B **716**, 1 (2012) [arXiv:1207.7214 [hep-ex]]; S. Chatrchyan *et al.* [CMS Collaboration], Phys. Lett. B **716**, 30 (2012) [arXiv:1207.7235 [hep-ex]].
 - [3] C. Englert, A. Freitas, M. M. Mühlleitner, T. Plehn, M. Rauch, M. Spira and K. Walz, J. Phys. G **41**, 113001 (2014) [arXiv:1403.7191 [hep-ph]]; for a comprehensive analysis of Run I data, including gauge boson production see e.g. A. Butter, O. J. P. Eboli, J. Gonzalez-Fraile, M. C. Gonzalez-Garcia, T. Plehn and M. Rauch, JHEP **1607**, 152 (2016) [arXiv:1604.03105 [hep-ph]].

- [4] for an independent estimate see e.g. M. Klute, R. Lafaye, T. Plehn, M. Rauch and D. Zerwas, *Europhys. Lett.* **101**, 51001 (2013) [arXiv:1301.1322 [hep-ph]].
- [5] A. Ball *et al*, Tech. Rep. FCC-ACC-SPC-0001.
- [6] <http://cepc.ihep.ac.cn/preCDR/volume.html>
- [7] R. Contino *et al.*, arXiv:1606.09408 [hep-ph].
- [8] T. Golling *et al.*, arXiv:1606.00947 [hep-ph].
- [9] M. Benedikt, talk at the FCC week 2015, Washington D.C., 23-29 March 2015, I. Hinchliffe, A. Kotwal, M. L. Mangano, C. Quigg and L. T. Wang, *Int. J. Mod. Phys. A* **30**, no. 23 (2015) [arXiv:1504.06108 [hep-ph]].
- [10] B. S. Acharya, K. Bozek, C. Pongkitivanichkul and K. Sakurai, *JHEP* **1502**, 181 (2015) [arXiv:1410.1532 [hep-ph]]; S. Gori, S. Jung, L. T. Wang and J. D. Wells, *JHEP* **1412**, 108 (2014) [arXiv:1410.6287 [hep-ph]]; J. Bramante, P. J. Fox, A. Martin, B. Ostdiek, T. Plehn, T. Schell and M. Takeuchi, *Phys. Rev. D* **91**, 054015 (2015) [arXiv:1412.4789 [hep-ph]]; A. Berlin, T. Lin, M. Low and L. T. Wang, *Phys. Rev. D* **91**, no. 11, 115002 (2015) [arXiv:1502.05044 [hep-ph]]; S. A. R. Ellis and B. Zheng, *Phys. Rev. D* **92**, no. 7, 075034 (2015) [arXiv:1506.02644 [hep-ph]].
- [11] J. Hajer, Y. Y. Li, T. Liu and J. F. H. Shiu, *JHEP* **1511**, 124 (2015) [arXiv:1504.07617 [hep-ph]]; A. Freitas, S. Westhoff and J. Zupan, *JHEP* **1509**, 015 (2015) [arXiv:1506.04149 [hep-ph]].
- [12] T. G. Rizzo, *Phys. Rev. D* **89**, no. 9, 095022 (2014) [arXiv:1403.5465 [hep-ph]]; A. Hook and A. Katz, *JHEP* **1409**, 175 (2014) [arXiv:1407.2607 [hep-ph]].
- [13] D. Curtin, P. Meade and C. T. Yu, *JHEP* **1411**, 127 (2014) [arXiv:1409.0005 [hep-ph]].
- [14] T. Han, J. Sayre and S. Westhoff, *JHEP* **1504**, 145 (2015) [arXiv:1411.2588 [hep-ph]]; M. L. Mangano, T. Plehn, P. Reimitz, T. Schell and H. S. Shao, *J. Phys. G* **43**, no. 3, 035001 (2016) [arXiv:1507.08169 [hep-ph]].
- [15] A. J. Barr, M. J. Dolan, C. Englert, D. E. Ferreira de Lima and M. Spannowsky, *JHEP* **1502**, 016 (2015) [arXiv:1412.7154 [hep-ph]]; A. V. Kotwal, S. Chekanov and M. Low, *Phys. Rev. D* **91**, no. 11, 114018 (2015) [arXiv:1504.08042 [hep-ph]]; W. Yao, arXiv:1308.6302 [hep-ph]; H. J. He, J. Ren and W. Yao, arXiv:1506.03302 [hep-ph]; A. Azatov, R. Contino, G. Panico and M. Son, *Phys. Rev. D* **92**, no. 3, 035001 (2015) [arXiv:1502.00539 [hep-ph]]; F. Kling, T. Plehn and P. Schichtel, arXiv:1607.07441 [hep-ph]; C. Englert, Q. Li, M. Spannowsky, M. Wang and L. Wang, arXiv:1702.01930 [hep-ph].
- [16] F. Bishara, R. Contino and J. Rojo, arXiv:1611.03860 [hep-ph].
- [17] D. Rainwater, arXiv:hep-ph/0702124; M. Rauch, arXiv:1610.08420 [hep-ph].
- [18] D. Rainwater, D. Zeppenfeld and K. Hagiwara, *Phys. Rev. D* **59**, 014037 (1999) T. Plehn, D. L. Rainwater and D. Zeppenfeld, *Phys. Rev. D* **61**, 093005 (2000) [arXiv:hep-ph/9911385].
- [19] D. Rainwater and D. Zeppenfeld, *Phys. Rev. D* **60**, 113004 (1999) [Erratum-ibid. *D* **61**, 099901 (2000)]; N. Kauer, T. Plehn, D. Rainwater and D. Zeppenfeld, *Phys. Lett. B* **503**, 113 (2001).
- [20] T. Han, G. Valencia and S. Willenbrock, *Phys. Rev. Lett.* **69**, 3274 (1992) [arXiv:hep-ph/9206246]; T. Figy, C. Oleari and D. Zeppenfeld, *Phys. Rev. D* **68**, 073005 (2003) [arXiv:hep-ph/0306109]; M. Ciccolini, A. Denner and S. Dittmaier, *Phys. Rev. D* **77**, 013002 (2008) [arXiv:0710.4749 [hep-ph]]; P. Bolzoni, F. Maltoni, S. O. Moch and M. Zaro, *Phys. Rev. Lett.* **105**, 011801 (2010) [arXiv:1003.4451 [hep-ph]]; M. Cacciari, F. A. Dreyer, A. Karlberg, G. P. Salam and G. Zanderighi, *Phys. Rev. Lett.* **115**, no. 8, 082002 (2015) [arXiv:1506.02660 [hep-ph]]; F. A. Dreyer and A. Karlberg, *Phys. Rev. Lett.* **117**, no. 7, 072001 (2016) [arXiv:1606.00840 [hep-ph]]; M. Rauch and S. Plätzer, [arXiv:1607.00159 [hep-ph]].
- [21] D. Zeppenfeld, R. Kinnunen, A. Nikitenko and E. Richter-Was, *Phys. Rev. D* **62**, 013009 (2000)
- [22] V. D. Barger, R. J. N. Phillips and D. Zeppenfeld, *Phys. Lett. B* **346**, 106 (1995) [arXiv:hep-ph/9412276]; D. L. Rainwater, R. Szalapski and D. Zeppenfeld, *Phys. Rev. D* **54**, 6680 (1996) [arXiv:hep-ph/9605444]; V. Del Duca *et al.*, *JHEP* **0610**, 016 (2006) [arXiv:hep-ph/0608158]; C. Bernaciak, M. S. A. Buschmann, A. Butter and T. Plehn, *Phys. Rev. D* **87**, 073014 (2013) [arXiv:1212.4436 [hep-ph]].
- [23] V. Silveira and A. Zee, *Phys. Lett. B* **161**, 136 (1985) J. McDonald, *Phys. Rev. D* **50**, 3637 (1994) [arXiv:hep-ph/0702143]; C. P. Burgess, M. Pospelov and T. ter Veldhuis, *Nucl. Phys. B* **619**, 709 (2001) [arXiv:hep-ph/0011335]; R. Schabinger and J. D. Wells, *Phys. Rev. D* **72**, 093007 (2005) [arXiv:hep-ph/0509209]; B. Patt and F. Wilczek, arXiv:hep-ph/0605188; R. Barbieri, T. Gregoire and L. J. Hall, arXiv:hep-ph/0509242; M. H. G. Tytgat, *PoSIDM* **2010**, 126 (2011) [arXiv:1012.0576 [hep-ph]]; C. Englert, T. Plehn, D. Zerwas and P. M. Zerwas, *Phys. Lett. B* **703**, 298 (2011) [arXiv:1106.3097 [hep-ph]].

- M. Pospelov and A. Ritz, Phys. Rev. D **84**, 113001 (2011) [arXiv:1109.4872 [hep-ph]]; X. -G. He and J. Tandean, Phys. Rev. D **84**, 075018 (2011) [arXiv:1109.1277 [hep-ph]]; P. J. Fox, R. Harnik, J. Kopp and Y. Tsai, Phys. Rev. D **85**, 056011 (2012) [arXiv:1109.4398 [hep-ph]]; I. Low, P. Schwaller, G. Shaughnessy and C. E. M. Wagner, Phys. Rev. D **85**, 015009 (2012) [arXiv:1110.4405 [hep-ph]]; C. Englert, T. Plehn, M. Rauch, D. Zerwas and P. M. Zerwas, Phys. Lett. B **707**, 512 (2012) [arXiv:1112.3007 [hep-ph]]; A. Djouadi, O. Lebedev, Y. Mambrini and J. Quevillon, Phys. Lett. B **709**, 65 (2012) [arXiv:1112.3299 [hep-ph]]; B. Batell, S. Gori and L. T. Wang, JHEP **1206**, 172 (2012) [arXiv:1112.5180 [hep-ph]]; S. Baek, P. Ko and W. I. Park, Phys. Rev. D **90**, no. 5, 055014 (2014) [arXiv:1405.3530 [hep-ph]].
- [24] A. Butter, T. Plehn, M. Rauch, D. Zerwas, S. Henrot-Versille and R. Lafaye, Phys. Rev. D **93**, 015011 (2016) [arXiv:1507.02288 [hep-ph]].
- [25] O. J. P. Eboli and D. Zeppenfeld, Phys. Lett. B **495**, 147 (2000) [arXiv:hep-ph/0009158].
- [26] C. Bernaciak, T. Plehn, P. Schichtel and J. Tattersall, Phys. Rev. D **91**, 035024 (2015) [arXiv:1411.7699 [hep-ph]].
- [27] G. T. Bodwin, F. Petriello, S. Stoynev and M. Velasco, Phys. Rev. D **88**, no. 5, 053003 (2013) [arXiv:1306.5770 [hep-ph]]; A. L. Kagan, G. Perez, F. Petriello, Y. Soreq, S. Stoynev and J. Zupan, Phys. Rev. Lett. **114**, no. 10, 101802 (2015) [arXiv:1406.1722 [hep-ph]]; M. König and M. Neubert, JHEP **1508**, 012 (2015) [arXiv:1505.03870 [hep-ph]]; I. Brivio, F. Goertz and G. Isidori, Phys. Rev. Lett. **115**, no. 21, 211801 (2015) [arXiv:1507.02916 [hep-ph]]; S. Alte, M. König and M. Neubert, arXiv:1609.06310 [hep-ph];
- [28] T. Plehn and D. Rainwater, Phys. Lett. B **520**, 108 (2001) K. Cranmer and T. Plehn, Eur. Phys. J. C **51**, 415 (2007) [arXiv:hep-ph/0605268]; see also T. Han and B. McElrath, Phys. Lett. B **528**, 81 (2002)
- [29] N. Kauer and G. Passarino, JHEP **1208**, 116 (2012) [arXiv:1206.4803 [hep-ph]]; F. Caola and K. Melnikov, Phys. Rev. D **88**, 054024 (2013) [arXiv:1307.4935 [hep-ph]]; J. M. Campbell, R. K. Ellis and C. Williams, JHEP **1404**, 060 (2014) [arXiv:1311.3589 [hep-ph]].
- [30] C. Englert and M. Spannowsky, Phys. Rev. D **90**, 053003 (2014) [arXiv:1405.0285 [hep-ph]]. G. Cacciapaglia, A. Deandrea, G. Drieu La Rochelle and J. B. Flament, Phys. Rev. Lett. **113**, no. 20, 201802 (2014) [arXiv:1406.1757 [hep-ph]]; A. Azatov, C. Grojean, A. Paul and E. Salvioni, Zh. Eksp. Teor. Fiz. **147**, 410 (2015) [J. Exp. Theor. Phys. **120**, 354 (2015)]; [arXiv:1406.6338 [hep-ph]].
- [31] T. Gleisberg, S. Höche, F. Krauss, M. Schönherr, S. Schumann, F. Siegert and J. Winter, JHEP **0902**, 007 (2009) [arXiv:0811.4622 [hep-ph]].
- [32] S. Catani, F. Krauss, R. Kuhn and B. R. Webber, JHEP **0111**, 063 (2001) [arXiv:hep-ph/0109231]; F. Krauss, JHEP **0208**, 015 (2002) [arXiv:hep-ph/0205283]; S. Höche, F. Krauss, S. Schumann and F. Siegert, JHEP **0905**, 053 (2009) [arXiv:0903.1219 [hep-ph]]; S. Höche, F. Krauss, M. Schönherr and F. Siegert, JHEP **1304**, 027 (2013) [arXiv:1207.5030 [hep-ph]].
- [33] M. Cacciari, G. P. Salam and G. Soyez, JHEP **0804**, 063 (2008) [arXiv:0802.1189 [hep-ph]]; M. Cacciari, G. P. Salam and G. Soyez, Eur. Phys. J. C **72**, 1896 (2012) [arXiv:1111.6097 [hep-ph]].
- [34] F. Cascioli, P. Maierhöfer and S. Pozzorini, Phys. Rev. Lett. **108**, 111601 (2012) [arXiv:1111.5206 [hep-ph]]; G. Ossola, C. G. Papadopoulos and R. Pittau, JHEP **0803**, 042 (2008) [arXiv:0711.3596 [hep-ph]]; A. van Hameren, Comput. Phys. Commun. **182**, 2427 (2011) [arXiv:1007.4716 [hep-ph]].
- [35] R. Kleiss and W. J. Stirling, Phys. Lett. B **200**, 193 (1988) U. Baur and E. W. N. Glover, Phys. Lett. B **252**, 683 (1990) V. D. Barger, K. m. Cheung, T. Han, J. Ohnemus and D. Zeppenfeld, Phys. Rev. D **44**, 1426 (1991) D. L. Rainwater, R. Szalapski and D. Zeppenfeld, Phys. Rev. D **54**, 6680 (1996) [arXiv:hep-ph/9605444]; B. E. Cox, J. R. Forshaw and A. D. Pilkington, Phys. Lett. B **696**, 87 (2011) [arXiv:1006.0986 [hep-ph]].
- [36] E. Gerwick, T. Plehn and S. Schumann, Phys. Rev. Lett. **108**, 032003 (2012) [arXiv:1108.3335 [hep-ph]].
- [37] S. Dawson, Nucl. Phys. B **249**, 42 (1985); G. L. Kane, W. W. Repko and W. B. Rolnick, Phys. Lett. B **148**, 367 (1984).
- [38] J. Brehmer, J. Jaeckel and T. Plehn, Phys. Rev. D **90**, no. 5, 054023 (2014) [arXiv:1404.5951 [hep-ph]]; see also P. Borel, R. Franceschini, R. Rattazzi and A. Wulzer, JHEP **1206**, 122 (2012) [arXiv:1202.1904 [hep-ph]].
- [39] S. D. Ellis, R. Kleiss and W. J. Stirling, Phys. Lett. **154B**, 435 (1985); F. A. Berends, W. T. Giele, H. Kuijf, R. Kleiss and W. J. Stirling, Phys. Lett. B **224**, 237 (1989); F. A. Berends, H. Kuijf, B. Tausk and W. T. Giele, Nucl. Phys. B **357**, 32 (1991); E. Gerwick, T. Plehn, S. Schumann and P. Schichtel, JHEP **1210**, 162 (2012) [arXiv:1208.3676 [hep-ph]].

- [40] T. Corbett, O. J. P. Eboli, D. Goncalves, J. Gonzalez-Fraile, T. Plehn and M. Rauch, JHEP **1508**, 156 (2015) [arXiv:1505.05516 [hep-ph]].
- [41] T. Plehn, D. L. Rainwater and D. Zeppenfeld, Phys. Rev. Lett. **88**, 051801 (2002) [arXiv:hep-ph/0105325]; G. Klamke and D. Zeppenfeld, JHEP **0704** (2007) 052 [arXiv:hep-ph/0703202]; K. Hagiwara, Q. Li and K. Mawatari, JHEP **0907**, 101 (2009) [arXiv:0905.4314 [hep-ph]]; C. Englert, D. Goncalves-Netto, K. Mawatari and T. Plehn, JHEP **1301**, 148 (2013) [arXiv:1212.0843 [hep-ph]]; C. Englert, D. Goncalves, G. Nail and M. Spannowsky, Phys. Rev. D **88**, 013016 (2013) [arXiv:1304.0033 [hep-ph]]; K. Hagiwara and S. Mukhopadhyay, JHEP **1305**, 019 (2013) [arXiv:1302.0960 [hep-ph]]; M. R. Buckley, T. Plehn and M. J. Ramsey-Musolf, Phys. Rev. D **90**, no. 1, 014046 (2014) [arXiv:1403.2726 [hep-ph]].
- [42] M. Buschmann, C. Englert, D. Goncalves, T. Plehn and M. Spannowsky, Phys. Rev. D **90**, no. 1, 013010 (2014) [arXiv:1405.7651 [hep-ph]].
- [43] M. Buschmann, D. Goncalves, S. Kuttimalai, M. Schönherr, F. Krauss and T. Plehn, JHEP **1502**, 038 (2015) [arXiv:1410.5806 [hep-ph]].
- [44] V. Khachatryan *et al.* [CMS Collaboration], Eur. Phys. J. C **75**, no. 5, 235 (2015) [arXiv:1408.3583 [hep-ex]].
- [45] S. Chatrchyan *et al.* [CMS Collaboration], JINST **7**, P10002 (2012) [arXiv:1206.4071 [physics.ins-det]]; G. Aad *et al.* [ATLAS Collaboration], Eur. Phys. J. C **76**, no. 5, 292 (2016) [arXiv:1603.05598 [hep-ex]].
- [46] CMS Collaboration, CMS-PAS-HIG-13-002 (2013) CMS Collaboration, Phys. Lett. B **736**, 64 (2014) [arXiv:1405.3455 [hep-ex]]; ATLAS collaboration, ATLAS-CONF-2014-042.
- [47] J. R. Andersen and J. M. Smillie, Phys. Rev. D **75**, 037301 (2007) [arXiv:hep-ph/0611281]; M. Ciccolini, A. Denner and S. Dittmaier, Phys. Rev. D **77**, 013002 (2008) [arXiv:0710.4749 [hep-ph]]; A. Bredenstein, K. Hagiwara and B. Jäger, Phys. Rev. D **77**, 073004 (2008) [arXiv:0801.4231 [hep-ph]].
- [48] J. Alwall, M. Herquet, F. Maltoni, O. Mattelaer and T. Stelzer, JHEP **1106**, 128 (2011) [arXiv:1106.0522 [hep-ph]].
- [49] T. Sjöstrand, S. Mrenna and P. Z. Skands, Comput. Phys. Commun. **178**, 852 (2008). [arXiv:0710.3820 [hep-ph]].
- [50] J. M. Campbell and R. K. Ellis, JHEP **1504**, 030 (2015) [arXiv:1502.02990 [hep-ph]].
- [51] B. W. Lee, C. Quigg and H. B. Thacker, Phys. Rev. D **16**, 1519 (1977).